Civil Engineering Dimension
https://ced.petra.ac.id

Effectiveness of Elastomeric Bearings in Reducing Pounding Effects between Reinforced Concrete Buildings under Seismic Condition

Rahman, M.R.A.[1], Saputra, A.[1]*, and Satyarno, I.[1]
[1] Department of Civil and Environmental Engineering, Gadjah Mada University
Jl. Grafika Kampus No. 2, Senolowo, Sinduadi, Mlati, Sleman, Yogyakarta 55284, INDONESIA

DOI: https://doi.org/10.9744/ced.27.1.47-58

Article Info:
Submitted: Sept 02, 2024
Reviewed: Oct 02, 2024
Accepted: Feb 15, 2025

Keywords:
pounding effect,
nonlinear time history,
RC frame structure,
elastomer bearing,
ETABS.

Corresponding Author:
Saputra, A.
Department of Civil and Environmental Engineering, Gadjah Mada University
Jl. Grafika Kampus No. 2, Senolowo, Sinduadi, Mlati, Sleman,
Yogyakarta 55284, INDONESIA
Email: saputra@ugm.ac.id

Abstract

This study investigates seismic pounding hazards between adjacent reinforced concrete buildings in East Java, particularly those designed under older regulations without pounding considerations. Nonlinear time history analysis was performed on three building models using eleven pairs of earthquake records scaled to SNI 8899:2020, representing Megathrust, Benioff, and Shallow Crustal earthquakes, with only three pairs analyzed in this study. Model 1 allowed free movement, Model 2 included concrete impact links with a 50 mm gap, and Model 3 utilized elastomer bearing links with a 9 mm gap. Results showed that elastomeric bearings reduced pounding forces by 81% to 95%, decreasing link force from 57437 kN to 5745 kN while withstanding axial loads up to 6276 kN, preventing collisions and maintaining structural stability. Additionally, Model 3 exhibited reduced floor accelerations and structural damage compared to Model 2, emphasizing the importance of elastomeric bearings in mitigating seismic pounding risks.

INTRODUCTION

The phenomenon of structural impact occurs when adjacent buildings collide during an earthquake, typically due to insufficient separation distance. This complex event can lead to severe outcomes, including wall damage, plastic deformation, shear failure of columns, and even structural collapse [1]. The collision between buildings often arises from differences in dynamic characteristics, inadequate spacing, or out-of-phase vibrations between adjacent structures [2]. Buildings with different floor elevations are particularly susceptible to impact during seismic events, as the additional shear forces on columns increase the risk of damage and instability. However, in urban areas, where buildings are constructed in close proximity due to financial and architectural constraints, such collisions are almost inevitable. The small or non-existent gaps between structures heighten the likelihood of interference and impact [3].

These interactions result in significant impact forces accompanied by short-duration acceleration spikes in each structure. The problem lies in the fact that these forces and accelerations are typically not considered in the structural design process. This means that each structure is designed independently to resist gravity and lateral loads, including seismic forces, without accounting for potential collisions. Consequently, improperly designed structures that are vulnerable to impact often suffer both local and global damage.

Structural impact can be classified into two types: floor-to-floor impact and floor-to-column impact. Floor-to-floor impact occurs when the slabs of adjacent buildings collide, especially if the structures are of the same height. Floor-

Note : Discussion is expected before July, 1st 2025, and will be published in the "Civil Engineering Dimension", volume 27, number 2, September 2025.
ISSN : 1410-9530 print / 1979-570X online
Published by : **Petra Christian University**

to-column impact occurs when the slab of one building collides with the column of another, typically when the floor levels of the two structures differ [4].

Structural impact has been recognized as a significant cause of building collapse in many earthquake events. During strong earthquakes, collisions can occur between closely situated buildings, particularly when there is little or no separation. These collisions can cause anything from minor local structural damage to severe structural failures [5].

Research on structural impact has been ongoing for over three decades. Several studies have explored the influence of dynamic properties and ground motion characteristics on the impact response of adjacent buildings. The impact effect becomes more significant when there are considerable differences in period, mass, or height between the structures [6]. The dynamic property differences between tall adjacent buildings can lead to structural impact during moderate to high-intensity earthquakes. This impact can impose additional forces on structural components, leading to damage or collapse, potentially resulting in loss of life [7]. Impact forces also affect the seismic behavior of structures, with collisions potentially causing regional damage to structural elements and leading to collapse. Studies indicate that these effects must be considered in structural design.

The most severe case of seismic impact occurred in Mexico in 1985, where collisions between adjacent buildings resulted in significant damage to 3 to 4.5% of the total damaged buildings. The extent of the damage was exacerbated by the absence of sufficient separation gaps or energy dissipation systems to accommodate relative movement between buildings [8].

METHOD

Physical Model for Interaction Between Adjacent Buildings

Reinforced concrete structures are widely utilized in civil engineering worldwide due to their strength, durability, and versatility in supporting various types of infrastructure, including buildings, bridges, and other essential public works. These structures are designed with various systems and structural patterns. Figure 1 presents the floor plan of the building, which will be modeled into three distinct variations. Model 1 represents the original structure, Model 2 assumes the occurrence of collisions between concrete elements, and Model 3 incorporates the addition of elastomeric bearing elements to the structure. Figure 2 shows Section B of the building, where link gap elements are assumed at the ends of the columns in both Model 2 and Model 3. The same assumption is applied in Sections A and C as well.

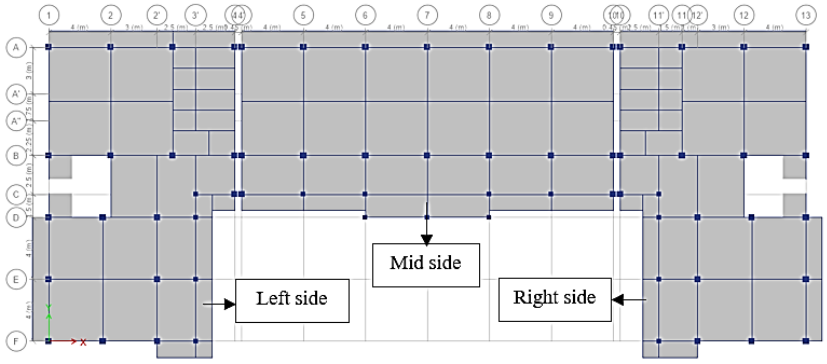

Figure 1. Plan of the Building

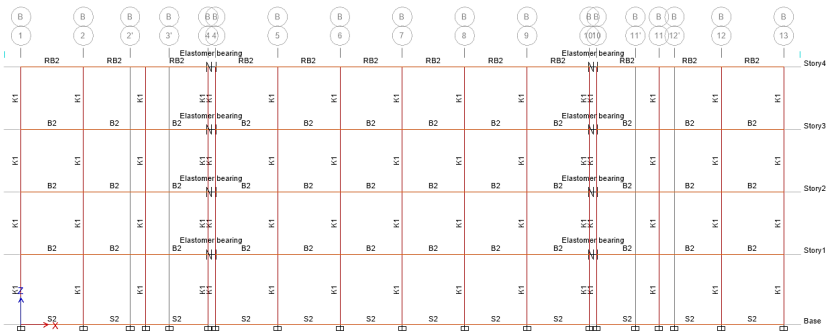

Figure 2. Section B

Table 1. Cross-sections and Reinforcement Ratio for Frames of All Buildings

Type		Dimension	Reinforcement	$\rho\%$
Column	K1	400×400	12D19	2.125
	K2	300×300	8D16	1.786
Beam	B1	500×250	8D16	1.286
	B1A	550×300	8D19	1.374
	B2	350×200	5D13	0.948
	B3	400×200	6D16	1.507
	B4	250×200	4D13	1.061
Ring beam	RB1	500×250	8D19	1.814
	RB2	350×200	7D16	2.010
	RB3	250×200	5D16	2.010
Sloof	S1	500×250	10D16	1.608
	S1A	550×300	12D16	1.137
	S2	350×200	6D13	1.137
	S3	300×200	4D13	0.884
	S4	200×150	4D12	1.507

The concrete used in these models has a compressive strength of $f'c = 20.75$ MPa, with an elastic modulus of $E = 21409$ MPa. The reinforcement steel used has a yield strength of $Fy = 420$ MPa and a Poisson's ratio of $v = 0.2$. Both dead loads (DL) and live loads (LL), including gravitational and lateral loads due to earthquakes, are considered in this analysis. Dead loads account for the self-weight of the structural components as well as additional dead loads on each component. Live loads are determined based on the function of the building's spaces by SNI 1727:2020. This building is classified as a risk category IV structure, functioning as an educational facility, and is located on a site classified as SD (medium soil). This structure consists of three adjacent buildings, with a spacing of 50 mm between each building. Each building comprises four stories, with the first floor measuring 4.5 meters in height and each subsequent floor measuring 4.0 meters. The floor slab thickness is 0.15 m, with cross-sections and rebar shown in Table 1.

Mathematical Modeling and Nonlinear Analysis Procedure

In this study, columns were modeled as fiber elements, while beam elements were modeled using plastic hinges. The nonlinear analysis accounted for structural deformation configurations, enabling the nonlinear force-deformation relationship to accurately capture material nonlinear behavior. The properties of plastic hinges were modeled based on the criteria outlined in ASCE 41-17, as the material elements and section properties allow for automatic plastic hinge modeling. The structure was modeled as an open frame, considering factors such as time constraints, hardware limitations, and the challenges in assessing the contribution of non-structural components to stiffness and lateral rigidity, as well as their impact on the moment-resisting frame system. Although non-structural components can increase the initial stiffness of the structure and reduce deformability, there are significant uncertainties and complexities in modeling the interaction between infill walls and the structural frame. As a result, this interaction is often neglected in the analysis [8].

Spectrum-Compatible Input Acceleration Time History

To get the structural response of the structure during and after seismic load excitation, time history analysis needs to be carried out. In this study, 11 earthquake records were selected as inputs for the analysis of nonlinear dynamic pounding effects. The selection of earthquake records was based on the location and characteristics of the building, as outlined in the Indonesian Seismic Hazard Deaggregation Map for Earthquake-Resistant Infrastructure Planning and Evaluation (2020). This process resulted in distance and magnitude constraints that can be used to find appropriate earthquake record data.

The acceleration records were adjusted to match the target site response spectrum using SeismoMatch software with a time-domain method. Ground motion history can be seen in Table 2. The selected earthquake records were scaled so that, for each period between $0{,}2T_{lower}$ dan $2T_{upper}$, the average 5% damped response spectrum for ground motion does not fall below the target response spectrum. T_{lower} represents the first period of the building when 90% mass participation is achieved, and T_{upper} is the fundamental period of the structural system [12].

Each pair of ground motion records must be modified so that the average response spectrum of the maximum direction is not less than 110% of the target response spectrum within the specified period range [14]. Due to software

limitations, the spectrum adjustment process did not use the rotD100 method but instead employed a standard adjustment method. Consequently, the compared value is the average response spectrum of all earthquake records against the target spectrum, calculated within a period range of 0.0716 seconds to 2.338 seconds. Figure 3(a) shows the original earthquake record, while Figure 3(b) presents the earthquake record adjusted to match the target response.

Table 2. Ground Motion History

No	Event/RSN	Year	Magnitude	Source	Distance (km)	Vs_{30} (m/s)	PGA (g)	D_{5-90}	Scale Factor
1	Tokachioki/ RSN4032547	2003	8.29	Megathrust	159.93	188.32	0.101	55.85	2.81
2	MiyagiPreOff/ RSN4016860	2011	7.15	Benioff	120.53	268.50	0.425	26.38	3.05
3	Tokachioki/ RSN4028554	2003	8.29	Megathrust	151.49	302.40	0.407	16.62	3.20
4	SouthSanriku/ RSN4028289	2003	7.03	Benioff	135.26	297.50	0.455	23.72	3.38
5	MiyagiPreOff/ RSN4007349	2011	7.15	Benioff	122.89	288.80	0.351	23.26	3.21
6	NorthernCalif01/ RSN8	1941	6.4	Shallow Crustal	44.68	219.31	0.272	15.5	3.66
7	Coalinga01/ RSN324	1983	6.36	Shallow Crustal	43.68	326.64	0.091	29	4.92
8	LomaPrieta/ RSN756	1989	6.93	Shallow Crustal	58.8	318.31	0.172	18.4	4.07
9	ChiChiTaiwan05/ RSN3222	1999	6.2	Shallow Crustal	60.33	223.04	0.300	16.1	3.99
10	ChiChiTaiwan06/ RSN3309	1999	6.3	Shallow Crustal	65.72	318.52	0.420	15.4	3.79
11	ChiChiTaiwan06/ RSN3265	1999	6.3	Shallow Crustal	40.33	277.5	0.130	16.6	2.78

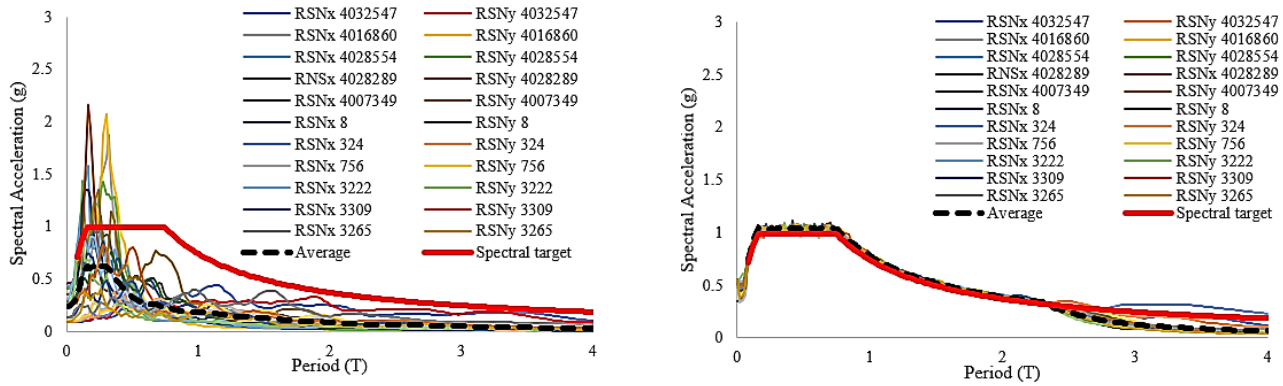

(a) Original response spectrum (b) Matched response spectrum

Figure 3. Response Spectrum

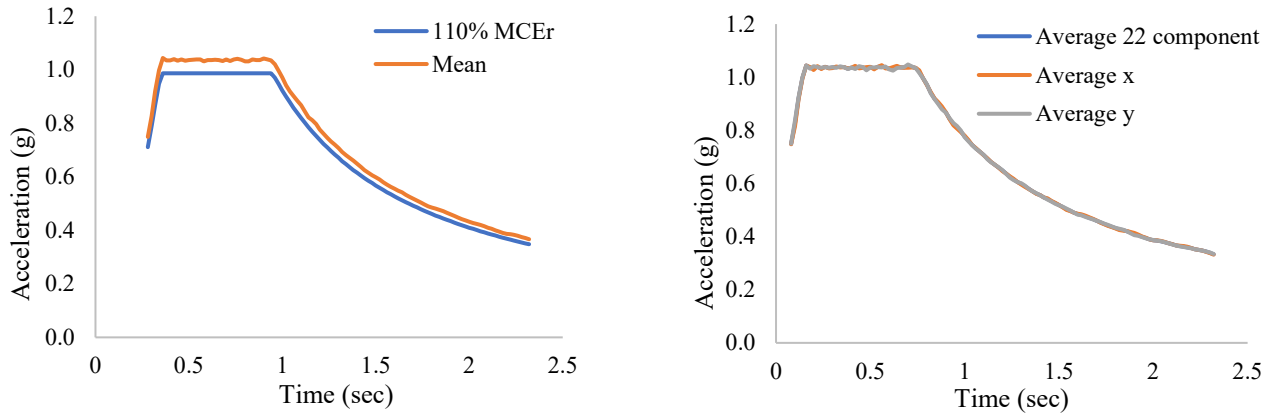

(a) Average Response Spectrum of All Earthquake Records (b) Average Spectrum of the Horizontal Components in the X and Y Directions

Figure 4. Average Response Spectrum of All Earthquake Records

Figure 4(a) shows that the average response spectrum of all earthquake records exceeds 110% of the target spectrum. Each pair of horizontal ground motion components must be applied to the building structure in orthogonal orientations, where the average spectrum of the horizontal components in the x and y directions (11 accelerogram components for each direction) must be within 10% of the average spectrum of all accelerogram components (22 components) [14]. As shown in Figure 4(b), the average spectrum of the horizontal components in the X and Y directions falls within the 10% limit of the overall component spectrum, with a maximum deviation of 1%.

Earthquake Records Used for Analysis

Among the 11 pairs of earthquake records that were adjusted, 3 pairs were selected for detailed analysis, with one pair representing each type: RSN 4032547 (Megathrust), RSN 4016860 (Benioff), and RSN 3309 (Shallow Crustal). The selection of these records was made due to time constraints associated with the computational demands of the nonlinear analysis.

The data input into ETABS consists of $D_{5\text{-}95}$ (significant duration) values, which specifically refer to the time duration between 5% and 95% of the total energy released during an earthquake. This approach is implemented to optimize processing time during the application run. The significant duration data was obtained using Prism software. The scaled earthquake records were input into Prism to extract the significant duration. The analysis results show that the significant duration of the Megathrust earthquake used in this study ranges from 53.44 seconds to 68.74 seconds, significantly affecting the dynamic response and structural deformation. The significant duration of the Benioff earthquake ranges from 28.99 seconds to 59.4 seconds, and for the Shallow Crustal earthquake, it ranges from 31.055 seconds to 46.14 seconds.

Structural Impact Model

ETABS provides various types of link elements. However, this study uses gap elements to simulate pounding, as these elements only activate under compressive forces. The separation distance between buildings is defined as the gap. The gap element generates axial forces when the gap is closed. The modeling of the gap using a nonlinear force-deformation relationship can be expressed by the following equation.

$$f = \begin{Bmatrix} K(d - open) \\ 0 \end{Bmatrix} \begin{matrix} if\ d - open < 0, \\ otherwise \end{matrix} \quad (1)$$

Where d represents displacement, $'open'$ refers to the gap width, which is always zero or positive, and K denotes the element stiffness. For the element K, impact stiffness can be determined as the lateral stiffness of the stiffer building. To evaluate the performance of gap elements, determining the appropriate separation distance between structures is crucial in the study of pounding effects. In a gap element, a clear space corresponding to the building separation must be maintained [13]. When two structures experience asymmetrical vibrations and approach each other closer than the designated separation, the stiffness of the element or the floor slabs begins to respond, generating a force within the element that is proportional to the pounding force experienced by the floor.

Introducing an adequate seismic gap between adjacent buildings not only reduces the risk of seismic pounding but can also eliminate it entirely. Research by Gong and Hao [15] concluded that the gap must be large enough to accommodate the maximum displacements of each building. Widening the seismic gap does not significantly affect pounding unless the buildings are adequately separated. However, this finding contrasts with Kamel's [16] results, which indicated that both the impact force and the number of collisions are highly sensitive to changes in the seismic gap distance. Overall, the research showed that increasing the seismic gap distance eightfold resulted in an average change in peak impact force by 32% and the number of collisions by 93%. This suggests that the number of collisions is more sensitive to seismic gap distance changes compared to peak impact force. Several previous studies have explored how to determine the stiffness of gap elements. A numerical simulation was conducted to identify the appropriate impact spring stiffness and the time interval for numerical integration according to wave propagation theory. It was concluded that the impact stiffness could be defined as the axial stiffness of the contacting bodies [9]. To calculate the impact stiffness of concrete for Model 2, the contact area (A) must first be determined. This value is obtained by multiplying the width and height of the column experiencing the impact, as shown in Model 1. The impacted column is Column K1, with a width of 400 mm. The width of the building experiencing a collision is b = 12000 mm. During the Megathrust earthquake, the largest displacement difference occurs on the top floor between the middle and right buildings at 4.40 seconds, with a value of 64.53 mm, as shown in Figure 5(a). The height of the

intersection point, measured from the building's base, is 4834 mm, as shown in Figure 5(b). The same approach is applied to the Shallow Crustal and Benioff earthquakes. During the Shallow Crustal earthquake, the intersection point height from the building's base was 6745 mm, while for the Benioff earthquake, it was 3227 mm.

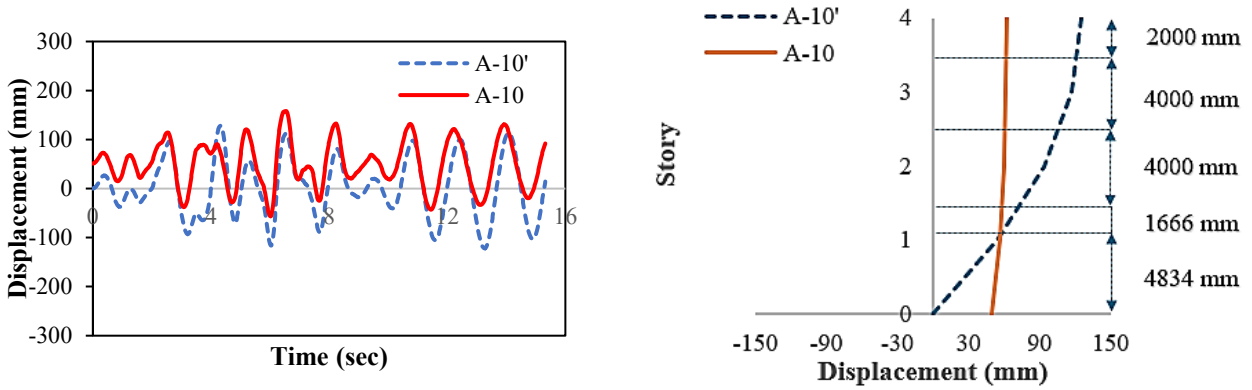

(a) 4-Story between the Mid and Right Side (b) Effective Height of Impact

Figure 5. Model 1 Displacement Graph for the Megathrust Earthquake

Each building possesses a rigid diaphragm, allowing the assumption that collisions occur between two rigid bodies. Therefore, the spring stiffness (K) should be greater than the sum of the axial stiffnesses of the colliding floors [10]. In analytical and experimental studies addressing the concrete-to-concrete impact, the spring stiffness is typically taken to be between approximately 10^4 kN/mm and 10^5 kN/mm [11]. In this study, the stiffness values were calculated using Equation (2).

$$K = \gamma \frac{EA}{b} \tag{2}$$

Where E represents the material's modulus of elasticity, A is the impact contact area, and b is the building's width in the direction of impact. The stiffness amplification factor $\gamma = 50$ was selected based on sensitivity analysis. This value was determined after considering several practical factors and supported by studies indicating that the system's response is not sensitive to changes in the stiffness of the impact elements [8]. Using this formula, the impact stiffness of concrete can be seen in Table 3.

Table 3. Assumed Impact Height and Stiffness in Model 2

Story	Megathrust		Shallow Crustal		Benioff	
	Height (mm)	Stiffness (kN/mm)	Height (mm)	Stiffness (kN/mm)	Height (mm)	Stiffness (kN/mm)
4	2000	71365	2000	71365	2000	71365
3	4000	142730	4000	142730	4000	142730
2	4000	142730	3755	133988	4000	142730
1	1666	59447	0	0	3273	116802

Table 4. Cross-sectional Data of the Elastomer Bearing used in Model 3

Nd [kN]	a [mm]	b [mm]	t [mm]	T_e [mm]	Weight [kg]	Kz [kN/mm]
6276	500	400	41	29	25.8	2151.4

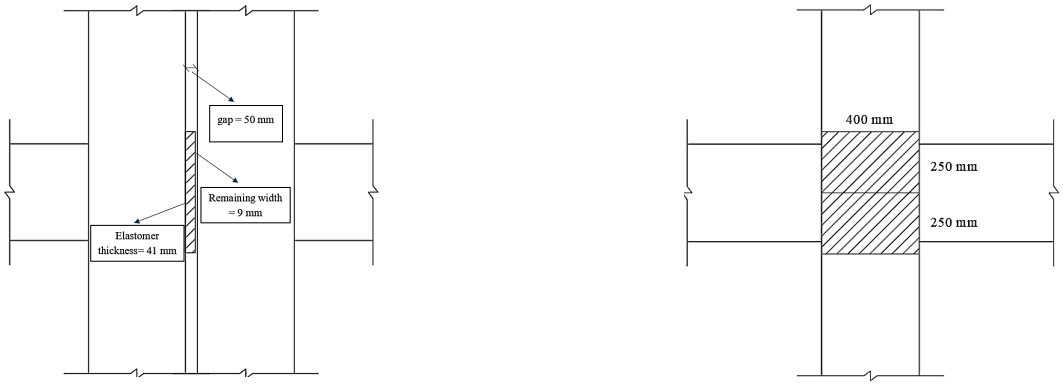

(a) B section (b) 4' section

Figure 6. Elastomer Bearing Configuration

Model 3 utilizes Lasto Block elastomer bearings as specified in Table 4. Two elastomer bearings, each measuring 250 x 400 x 41 mm, are arranged in parallel on either side of the column subject to impact in Figure 6. The use of these two elastomer bearings increases the total stiffness to 2151.4 kN/mm and the bearing capacity to 6276 kN. The selection of this size was based on multiple trials until the final result showed that the bearing capacity could adequately withstand the axial forces encountered.

RESULTS AND DISCUSSION

Pounding Forces

In Figure 7, it can be observed that the use of elastomeric bearings during a Megathrust earthquake is able to reduce axial forces by approximately 81% on the left building pounding and 88% on the right building pounding. In Figure 8, it can be seen that the use of elastomeric bearings during a Shallow Crustal earthquake reduces axial forces by about 95% on the left building pounding and 84% on the right building pounding. In Figure 9, it is shown that the use of elastomeric bearings during a Benioff earthquake reduces axial forces by approximately 82% on the left building pounding and 95% on the right building pounding. The following table provides a comparison of the pounding values.

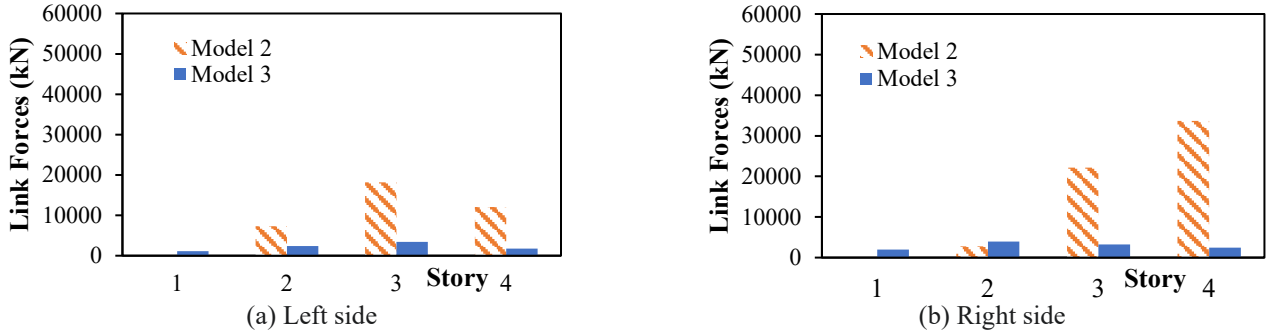

Figure 7. Maximum Pounding Force Response Time Histories during Megathrust Earthquake

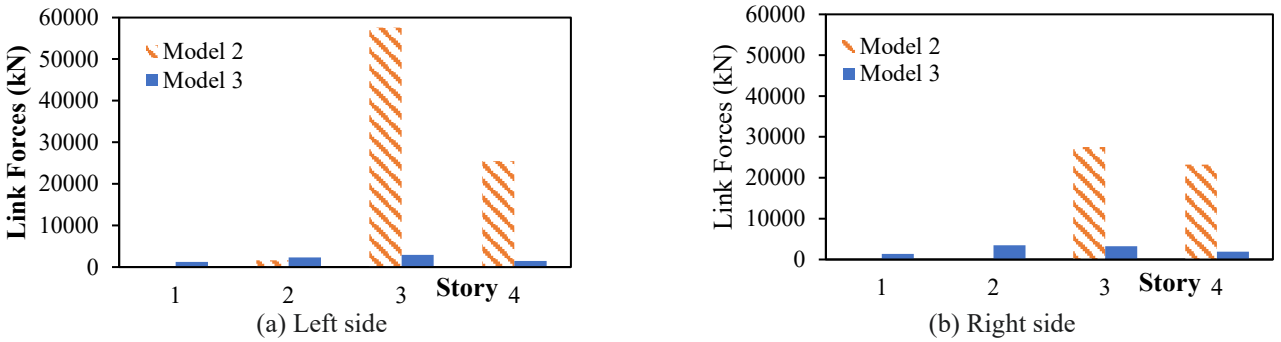

Figure 8. Maximum Pounding Force Response Time Histories during Shallow Crustal Earthquake

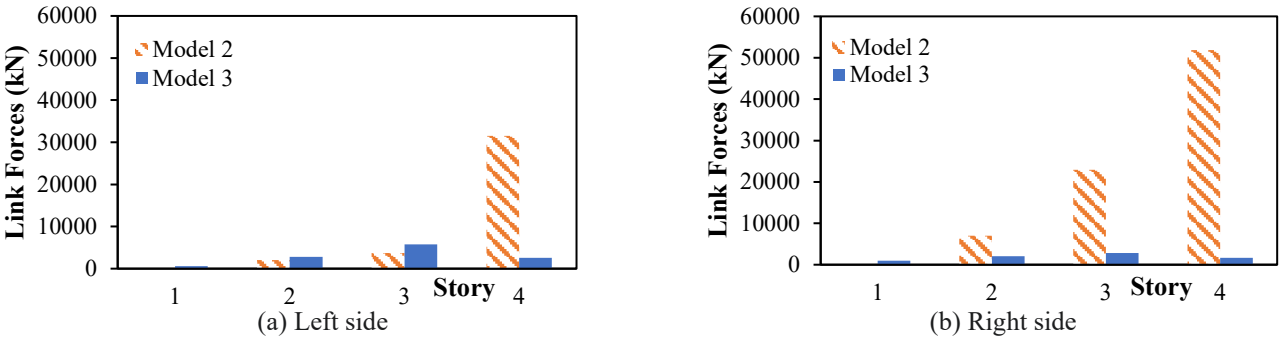

Figure 9. Maximum Pounding Force Response Time Histories during Benioff Earthquake

Table 5 and Table 6 present the maximum pounding forces at each floor level for different types of earthquakes on the left and right side of the building. In Model 2, the highest pounding force recorded was 57547 kN during the

Shallow Crustal earthquake, whereas in Model 3, the maximum pounding force was 5745 kN during the Benioff earthquake.

Table 5. Peak Pounding Forces Induced at Different Story Levels on the Left Side

Story	Megathrust		Shallow Crustal		Benioff	
	Model 2 Pounding (kN)	Model 3 Pounding (kN)	Model 2 Pounding (kN)	Model 3 Pounding (kN)	Model 2 Pounding (kN)	Model 3 Pounding (kN)
Story 1	0	1139	0	1234	0	567
Story 2	7329	2419	1613	2328	2021	2813
Story 3	18205	3407	57547	2928	3687	5745
Story 4	12064	1768	25475	1462	31543	2608

Table 6. Peak Pounding Forces Induced at Different Story Levels on the Right Side

Story	Megathrust		Shallow Crustal		Benioff	
	Model 2 Pounding (kN)	Model 3 Pounding (kN)	Model 2 Pounding (kN)	Model 3 Pounding (kN)	Model 2 Pounding (kN)	Model 3 Pounding (kN)
Story 1	0	2017	0	1370	0	957
Story 2	2783	3952	0	3485	7018	2027
Story 3	22166	3243	27528	3243	22952	2785
Story 4	33704	2463	23246	1887	51879	1660

Intersection of the Peak Floor

Figure 10, Figure 11, and Figure 12 illustrate the displacement overtime on the 4th floor of the building during a Megathrust earthquake. The graphs indicate that each model exhibits different displacement behaviors due to variations in the assumptions used. In Model 1, it is assumed that the buildings lack any linkage, allowing each building to move independently without mutual influence. The graph shows intersecting lines, indicating potential collision effects at these points. In Model 2, it is assumed that the buildings are connected by links with a certain stiffness, allowing for concrete collisions between buildings and resulting in impact forces, thus affecting each other. This model shows points of contact at several locations, indicating impacts between the buildings rather than intersecting lines. In Model 3, it is assumed that the buildings are equipped with elastomeric bearings with stiffness according to the specifications provided in the elastomeric bearing catalog. There is no intersecting or touching lines are observed, demonstrating the absence of collisions between buildings due to the elastomeric bearings installed in the gaps between buildings.

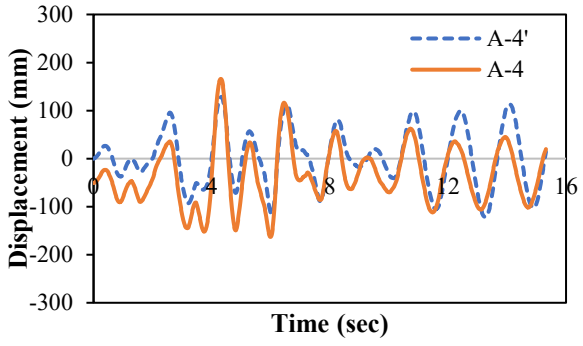

(a) 4-Story between the Left and Mid-side

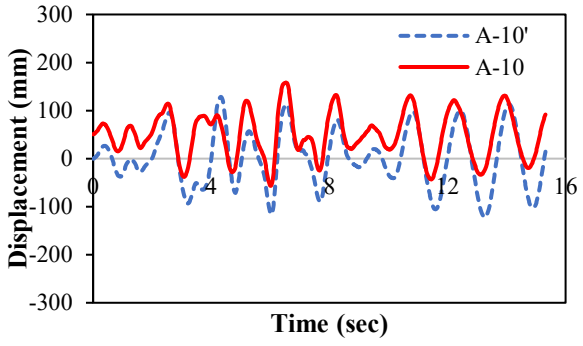

(b) 4-Story between the Mid and Right-side

Figure 10. Longitudinal Displacement Time Histories for Different in-plan Alignments during the Megathrust Earthquake in Model 1

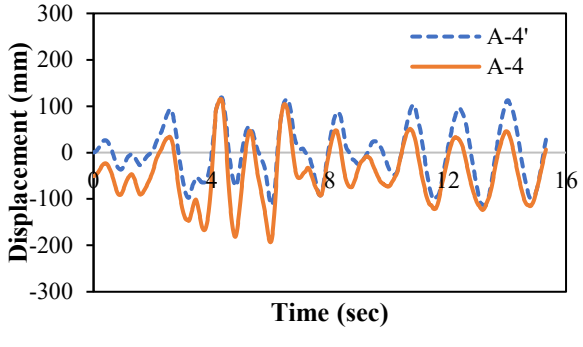

(a) 4-Story between the Left and Mid-side

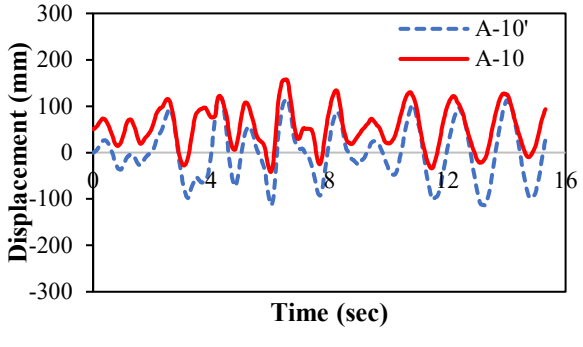

(b) 4-Story between the Mid and Right-side

Figure 11. Longitudinal Displacement Time Histories for Different In-plan Alignments during the Megathrust Earthquake in Model 2

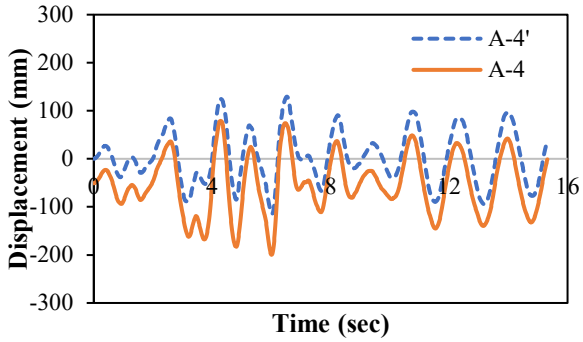

(a) 4-Story between the Left and Mid-side

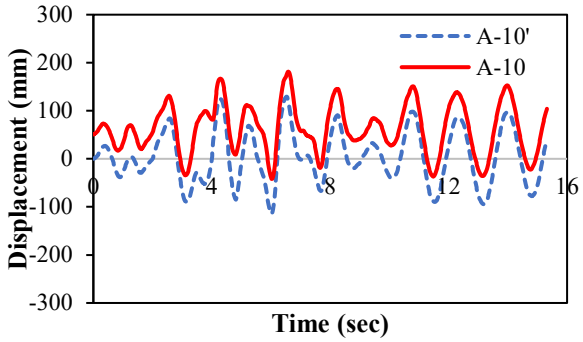

(b) 4-Story between the Mid and Right-side

Figure 12. Longitudinal Displacement Time Histories for Different In-plan Alignments during the Megathrust Earthquake in Model 3

Total Step Distribution by State

Table 7. Comparison of Total Steps across States for Different Models at Column K1 in Grid B-4 under the Megathrust Earthquake

State	Step											
	Story 1			Story 2			Story 3			Story 4		
	Model			Model			Model			Model		
	1	2	3	1	2	3	1	2	3	1	2	3
A-B	235	235	238	1533	635	1533	1533	1533	1533	1533	616	1533
B-C	107	183	1295	0	898	0	0	0	0	0	917	0
C-D	0	235	0	0	0	0	0	0	0	0	0	0
D-E	0	0	0	0	0	0	0	0	0	0	0	0
>E	1191	880	0	0	0	0	0	0	0	0	0	0
Total Step	1533	1533	1533	1533	1533	1533	1533	1533	1533	1533	1533	1533

Table 8. Comparison of Total Steps across States for Different Models at Column K1 in Grid B-4 under the Shallow Crustal Earthquake

State	Step											
	Story 1			Story 2			Story 3			Story 4		
	Model			Model			Model			Model		
	1	2	3	1	2	3	1	2	3	1	2	3
A-B	560	561	561	3023	2132	3023	3023	3023	3023	3023	3023	3023
B-C	142	144	139	0	891	0	0	0	0	0	0	0
C-D	0	0	0	0	0	0	0	0	0	0	0	0
D-E	0	0	0	0	0	0	0	0	0	0	0	0
>E	2321	2318	2323	0	0	0	0	0	0	0	0	0
Total Step	3023	3023	3023	3023	3023	3023	3023	3023	3023	3023	3023	3023

Table 9. Comparison of Total Steps across States for Different Models at Column K1 in Grid B-4 under the Benioff Earthquake

State	Step											
	Story 1			Story 2			Story 3			Story 4		
	Model			Model			Model			Model		
	1	2	3	1	2	3	1	2	3	1	2	3
A-B	102	102	101	344	344	345	2594	2594	2594	2594	441	2594
B-C	235	235	237	2250	2250	2249	0	0	0	0	2153	0
C-D	0	0	0	0	0	0	0	0	0	0	0	0
D-E	0	0	0	0	0	0	0	0	0	0	0	0
>E	2257	2257	2256	0	0	0	0	0	0	0	0	0
Total Step	2594	2594	2594	2594	2594	2594	2594	2594	2594	2594	2594	2594

Table 7, Table 8, and Table 9 compare the total steps based on the state at Column K1 in Grid B-4 under Megathrust, Shallow Crustal, and Benioff earthquakes, respectively. State A-B represents the elastic condition, B-C indicates initial cracking, C-D denotes advanced cracking or permanent deformation, D-E signifies severe damage, and state >E represents total collapse. Structural damage analysis based on state damage reveals that Model 1 experienced more severe damage (state >E) in Story 1 during Megathrust and Shallow Crustal earthquakes compared to Models 2 and 3, indicating that even without collisions, inertial forces were concentrated at the lower stories. Model 2

exhibited more distributed damage across stories during certain earthquakes, with less severe damage in Story 1 compared to Model 1, as indicated by fewer steps in state >E. This is attributed to the uneven distribution of collision energy, which was more intense in upper stories such as Story 2 or Story 4. In contrast, Model 3 effectively mitigated collision energy using elastomer bearings, resulting in reduced damage across all stories compared to Models 1 and 2. The collision energy in Model 2 caused localized dynamic force concentrations, leading to greater damage in Story 2 during Shallow Crustal earthquakes and Story 4 during Benioff earthquakes. While Model 2 exhibits significant damage in certain stories (e.g., Story 2 and Story 4), the reduced steps in state >E for Story 1 indicate that the collision forces redistribute energy more rapidly, leading to varying damage patterns across the structure.

Deformation Patterns in Grid B

Figure 13 illustrates the elevation view of the building in Grid B during the Megathrust earthquake for Models 1, 2, and 3 at step 1532. In Model 1, the building exhibits a uniform deformation pattern, primarily influenced by inertial forces, with no additional interaction between structural elements. In contrast, Model 2 shows significant deformation and irregularities due to the collision forces, particularly at certain stories, highlighting the uneven redistribution of energy during the seismic event. Model 3 demonstrates reduced deformation compared to Model 2, as the elastomer bearings effectively absorb collision energy and minimize its transmission to the structure. These visual comparisons confirm that while Model 2 experiences more localized damage due to collisions, Model 3 provides improved overall structural performance by mitigating the effects of collisions.

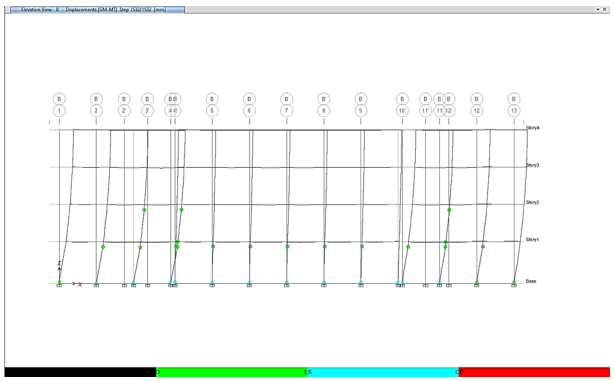

(a) Model 1

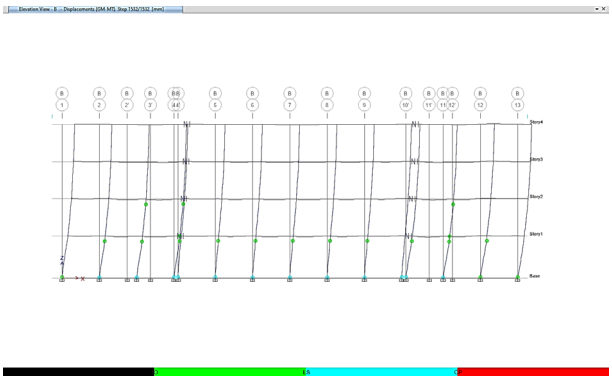

(b) Model 2

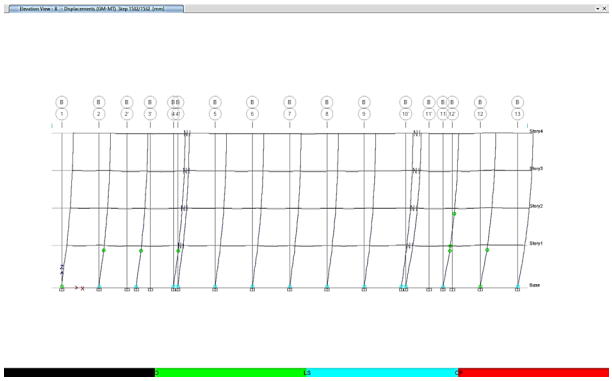

(b) Model 3

Figure 13. Elevation View of the Building in Grid B during Megathrust Earthquake

Floor Acceleration

Floor accelerations represent the dynamic responses of the buildings to seismic events. Table 10 presents the maximum acceleration values at point C-10 for various earthquake types. In Model 1, the maximum accelerations due to the Megathrust, Shallow Crustal, and Benioff earthquakes were 7.03 m/s², 6.74 m/s², and 6.73 m/s², respectively. In Model 2, accelerations surged dramatically, reaching 523.49 m/s² (Megathrust), 937.97 m/s² (Shallow Crustal), and 164.88 m/s² (Benioff) due to collisions between rigid concrete elements. In Model 3, the accelerations were effectively reduced to 35.14 m/s², 44.87 m/s², and 65.89 m/s², respectively. The significant floor acceleration in Model 2 resulted in non-structural damage to the building. The elastomer bearings absorbed collision energy, significantly lowering the transmitted accelerations to the structure, although not completely eliminating the effects.

Table 10. Maximum Floor Acceleration obtained at Point C-10

Floor	Acceleration (m/s^2)								
	Megathrust			Shallow Crustal			Benioff		
	Model			Model			Model		
	1	2	3	1	2	3	1	2	3
Story 1	4.05	3.90	11.82	3.72	3.75	8.38	3.98	4.06	11.43
Story 2	6.01	67.58	21.77	5.29	12.29	15.12	4.40	28.71	19.00
Story 3	6.96	151.68	18.78	6.33	79.28	25.28	5.77	131.64	35.32
Story 4	7.03	523.49	35.14	6.74	937.97	44.87	6.73	164.88	65.89

CONCLUSIONS

Based on the research that was done, it can be concluded as follows:

1. The use of elastomer bearings has proven to be highly effective in reducing impact forces (link forces) by 81% to 95% across various types of earthquakes.
2. Two elastomer bearings installed in parallel have a capacity of 6276 kN, while the maximum pounding forces recorded during the Megathrust earthquake for Model 3 were 3952 kN, 3485 kN for the Shallow Crustal earthquake, and 5745 kN for the Benioff earthquake. Therefore, the elastomer bearings are capable of withstanding the impact forces generated.
3. Elastomer bearings were also successful in preventing collisions between buildings (replacing building-to-building collisions with building-to-bearing collisions).
4. The study demonstrates that while collisions in Model 2 significantly amplify floor accelerations, causing non-structural damage, the use of elastomer bearings in Model 3 effectively mitigates these accelerations by absorbing collision energy, reducing seismic impact on the structure.
5. The analysis reveals that Model 2 experiences significantly greater structural damage across multiple floors due to large collisions, whereas Model 3 with elastomer bearings effectively mitigates such damage compared to Model 1 without collisions.
6. Overall, elastomer bearings are an effective and reliable solution for mitigating inter-building impact forces.

REFERENCES

1. Hammid, M., Rahman, F.U., and Ali, Q., Effects of Pounding on the Behavior of Reinforced Concrete Frame Structures in Seismic Zone 2B, *Journal of Engineering Research*, *10*(4B), 2021, pp. 99–114.
2. Naderpour, H., Barros, R.C., Khatami, S.M., and Jankowski, R., Numerical Study on Pounding between Two Adjacent Buildings under Earthquake Excitation, *Shock and Vibration*, 2016, http://dx.doi.org/10.1155/2016/1504783.
3. Elgammal, A., Seleemah, A., Elsharkawy, M., and Elwardany, H., Comprehensive Review on Seismic Pounding Between Adjacent Buildings and Available Mitigation Measures, *Archives of Computational Methods in Engineering*, *31*, 2024, pp. 1–36, https://doi.org/10.1007/s11831-024-10114-6.
4. Miari, M. and Jankowski, R., Analysis of Floor-to-Column Pounding of Buildings Founded on Different Soil Types, *Bulletin of Earthquake Engineering*, *20*, 2022, pp. 7241–7262, https://doi.org/10.1007/s10518-022-01482-0.
5. Polycarpou, C.P., Papaloizou, L., Komodromos, P., and Charmpis, C.D., Effect of the Seismic Excitation Angle on the Dynamic Response of Adjacent Buildings during Pounding, *Earthquakes and Structures*, *8*(5), 2015, pp. 1127–1146, http://dx.doi.org/10.12989/eas.2015.8.5.1127.
6. Miari, M. and Jankowski, R., Analysis of Pounding between Adjacent Buildings Founded on Different Soil Types, *Soil Dynamics and Earthquake Engineering*, *154*, 2022, https://doi.org/10.1016/j.soildyn.2022.107156.
7. Kumar, M.P. and Kumar, J.D.C., Seismic Pounding of the Adjacent Buildings with Different Heights, *International Journal of Engineering Research and Science & Technology*, *4*(4), 2015.
8. Raheem, S.E.A., Fooly, M.Y.M., Omar, M., and Zaher, A.K.A., Seismic Pounding Effects on the Adjacent Symmetric Buildings with Eccentric Alignment, *Earthquakes and Structures*, *16*(6), 2019, pp. 715–726, https://doi.org/10.12989/eas.2019.16.6.715.
9. Watanabe, G. and Kawashima, K., Numerical Simulation of Pounding of Bridge Decks, *Proceedings of the 13th World Conference on Earthquake Engineering*, 2004, pp. 1–6.
10. Ozer, E., Seismic Pounding of Adjacent Buildings Considering Torsional Effects, *Bulletin of Earthquake Engineering*, *22*, 2024, pp. 2139–2171, https://doi.org/10.1007/s10518-023-01849-x.

11. Ghandil, M. and Aldaikh, H., Damage-based Seismic Planar Pounding Analysis of Adjacent Symmetric Buildings Considering Inelastic Structure–Soil–Structure Interaction, *Earthquake Engineering and Structural Dynamics*, *46*(7), 2016, pp. 1141–1159, https://doi.org/10.1002/eqe.2848.
12. SNI 1726:2019, *Tata Cara Perencanaan Ketahanan Gempa untuk Struktur Bangunan Gedung dan Non Gedung*, Badan Standardisasi Nasional, Jakarta, 2019.
13. Naseri, S.A., Amiri, J.V., Rajabnejad, H., and Sadeghi, A., A Study into the Effect of Different Ground Motion Durations on the Seismic Pounding Force by Considering Soil-Structure Interaction, *Asian Journal of Civil Engineering*, *23*, 2022, pp. 53–65, https://doi.org/10.1007/s42107-021-00408-6.
14. SNI 8899:2020, *Tata Cara Pemilihan dan Modifikasi Gerak Tanah Permukaan untuk Perencanaan Gedung Tahan Gempa*, Badan Standardisasi Nasional, Jakarta, 2020.
15. Gong, L. and Hao, H., Analysis of Coupled Lateral-Torsional Pounding Responses of One-Story Asymmetric Adjacent Structures Subjected to Bi-Directional Ground Motions Part I: Uniform Ground Motion Input, *Advances in Structural Engineering*, *8*(5), 2005, pp. 463–479, https://doi.org/10.1260/136943305774858043.
16. Kamel, K.T., Estimating the Seismic Pounding Force between Adjacent Buildings and Study the Effect of Gap Distance on Seismic Pounding, *Asian Journal of Civil Engineering*, *24*, 2022, pp. 153–167, https://doi.org/10.1007/s42107-022-00494-0.